Giant spin Hall effect in perpendicularly spin-polarized FePt/Au devices

TAKESHI SEKI[1]*, YU HASEGAWA[1], SEIJI MITANI[1], SABURO TAKAHASHI[1,2], HIROSHI IMAMURA[2,3], SADAMICHI MAEKAWA[1,2], JUNSAKU NITTA[4] AND KOKI TAKANASHI[1]

[1]Institute for Materials Research, Tohoku University, Sendai 980-8577, Japan
[2]CREST, Japan Science and Technology Agency, Tokyo 102-0075, Japan
[3]National Institute of Advanced Industrial Science and Technology, Tsukuba 305-8568, Japan
[4]Graduate School of Engineering, Tohoku University, Sendai 980-8579, Japan
*e-mail: go-sai@imr.tohoku.ac.jp

Published online: 13 January 2008; doi:10.1038/nmat2098

Conversion of charge current into pure spin current and vice versa in non-magnetic semiconductors[1–5] or metals[6–8], which are called the direct and inverse spin Hall effects[9–16] (SHEs), provide a new functionality of materials for future spin-electronic architectures[17]. Thus, the realization of a large SHE in a device with a simple and practical geometry is a crucial issue for its applications. Here, we present a multi-terminal device with a Au Hall cross and an FePt perpendicular spin injector to detect giant direct and inverse SHEs at room temperature. Perpendicularly magnetized FePt injects or detects perpendicularly polarized spin current without magnetic field, enabling the unambiguous identification of SHEs. The unprecedentedly large spin Hall resistance of up to 2.9 mΩ is attributed to the large spin Hall angle in Au through the skew scattering mechanism and the highly efficient spin injection due to the well-matched spin resistances of the chosen materials.

The origin of the spin Hall effect (SHE) is believed to be similar to that of the anomalous Hall effect (AHE) in ferromagnetic materials with spontaneous magnetization. According to theories of the AHE[18], one of its origins is spin–orbit scattering of conduction electrons through skew and/or side-jump scattering by non-magnetic impurities, or through spin-disordered scattering[19]. A key to obtaining a large Hall angle (α_H) is a large spin–orbit coupling parameter (η_{so}). The most distinguished point of the SHE is that it does not require ferromagnetic order. When an unpolarized charge current flows in a non-magnetic material with a large η_{so}, up- and down-spin electrons are scattered in opposite directions, thus generating a pure spin current in the transverse direction (without an accompanying charge current), which is called the direct SHE (DSHE). On the other hand, the flow of a spin current in the same material induces a transverse charge current, which is referred to as the inverse SHE (ISHE).

Theoretical studies based on the skew and/or side-jump scattering mechanisms[10,11,15] and on the distinctive band structure in the presence of spin–orbit coupling[12,13] and experimental studies on optically detected SHE in non-magnetic semiconductors such as GaAs (refs 1–4) and ZnSe (ref. 5) have stimulated much scientific interest and have raised the possibility of SHE-based devices. More recently, in non-magnetic metals such as Pt (refs 7,8) or Al (ref. 6), the SHE has been electrically detected by using the non-local spin-injection or spin-pumping technique. Pt is a well-known non-magnetic metal with a large η_{so}, and, indeed, a room-temperature SHE has been detected. However, its short spin diffusion length (λ_N) makes it very difficult to observe the SHE, so sophisticated device structures[8] or measurement techniques[7] are required. Al shows a relatively long λ_N but a quite small η_{so}; therefore, the small ISHE is observed only at low temperature. In addition, a perpendicular magnetic field larger than the in-plane demagnetizing field is needed to magnetize a spin injector perpendicular to the film plane[6].

We fabricated a multi-terminal device consisting of a Au Hall cross and an FePt perpendicular spin injector as shown schematically in Fig. 1a. Au is a non-magnetic metal with a large η_{so} and a simple electronic structure. The FePt spin injector with perpendicular magnetization generates perpendicularly (z directionally) polarized spin current flowing in the positive x direction without a perpendicular magnetic field. The spin current is deflected at the Au Hall cross, and charge accumulation occurs in the y direction, which is detected as the Hall voltage. The widths of the Hall cross and the spin injector are 150 nm and 200 nm, respectively, and the distance from the edge of the spin injector to that of the Hall cross (d) is varied in the range from 70 nm to 400 nm (Fig. 1b). The resistivities (ρ) of Au and FePt at 295 K are 2.7 μΩ cm and 36 μΩ cm, respectively.

An advantage of the present multi-terminal device is that three kinds of Hall effect, that is, DSHE, ISHE and local Hall effect (LHE), are measured in the same device by simply changing the terminal configuration of the bias current (I) and the voltmeter. When I flows from terminal A to B, I^{A-B}, and the voltage (V) is measured between terminals C and D, V^{C-D}, the terminal configuration corresponds to the ISHE geometry. The resistance of the ISHE ($R_{ISHE} = V^{C-D}/I^{A-B}$) versus magnetic field (H) applied in the z direction is shown in Fig. 1c. For comparison, the hysteresis loop of the resistance of the LHE ($R_{LHE} = V^{B-C}/I^{A-F}$) is also shown. The shape of the hysteresis loop of R_{ISHE} obtained at 295 K is the same as that of R_{LHE}. The LHE mainly originates from the AHE in FePt, indicating that the change of R_{ISHE} reflects the magnetization reversal of FePt. The voltage change of the ISHE ($\Delta V = V_\uparrow - V_\downarrow$) varies linearly with I, where $V_\uparrow$ and $V_\downarrow$ are the voltages when the magnetic moment of FePt points upward and downward, respectively. From the absolute value of ΔV versus I, the resistance change of the ISHE (ΔR_{ISHE}) is found to be

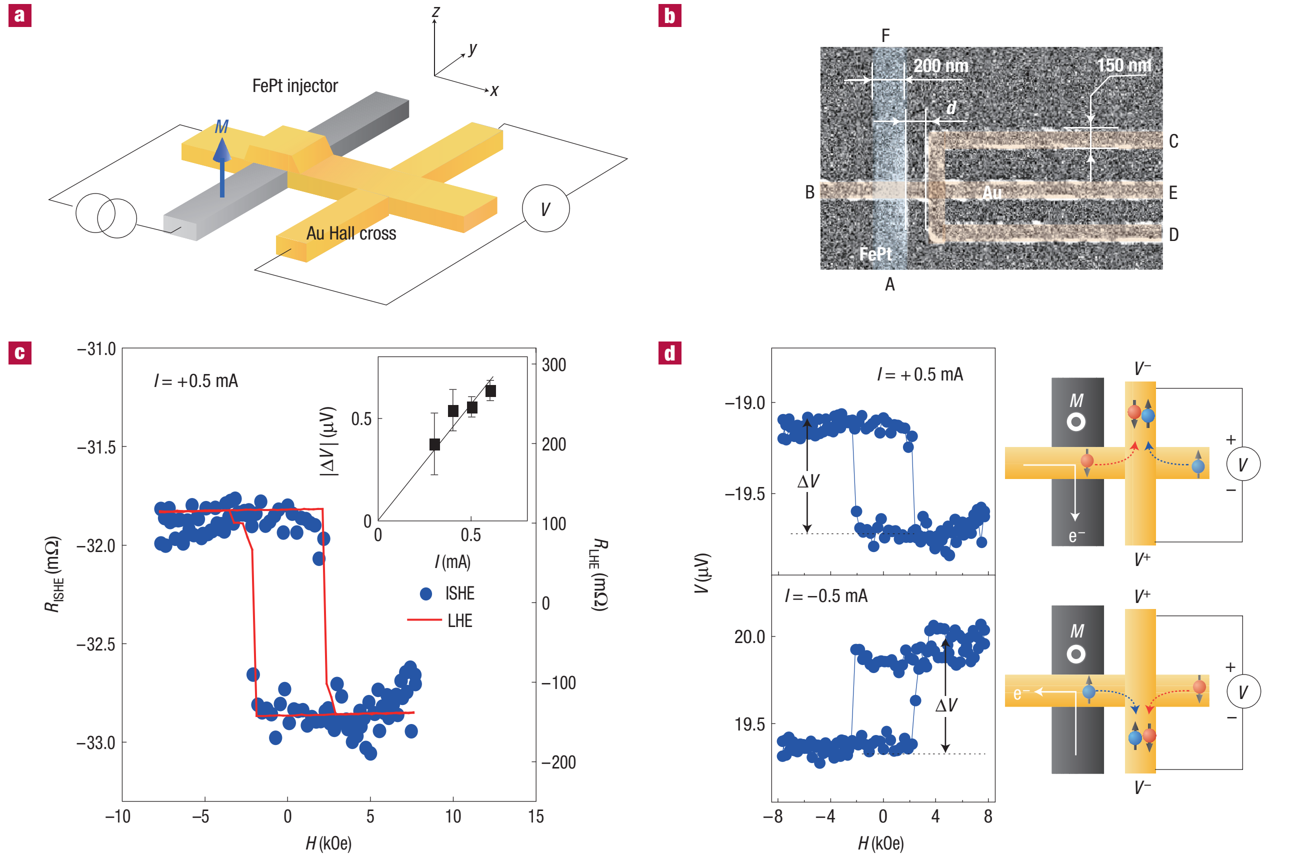

Figure 1 **ISHE. a**, Schematic diagram of the multi-terminal device consisting of the Au Hall cross and the FePt perpendicular spin injector. The current source and the voltmeter are configured for the detection of ISHE. **b**, Scanning electron microscope image of the device. The widths of the Au Hall cross and the FePt spin injector are 150 nm and 200 nm, and their thicknesses are 10 nm. The distance between the edges of the Au Hall cross and the FePt spin injector d is varied in the range from 70 nm to 400 nm. The capital letters represent the terminal positions for the measurement. **c**, Resistance of ISHE geometry R_{ISHE} versus external magnetic field H for the device with $d = 150$ nm superimposed on the resistance of the local Hall geometry R_{LHE} (red lines). The measurement is carried out at 295 K. Inset: Absolute value of voltage change $|\Delta V|$ versus bias current I. The error bars are due to the scattered data points in the R_{ISHE}–H curves. **d**, V versus H of ISHE for $I = +0.5$ mA and -0.5 mA (left panels). The corresponding diagrams (right panels) explain the relationship between the electron flow direction and the voltage polarities where the FePt spin injector shows upward magnetization at positive H. The moments of conduction electron spins are denoted by blue (majority spin) and red (minority spin) symbols.

1.15 mΩ. Although the magnitude of ΔV for $I = +0.5$ mA is equal to that for $I = -0.5$ mA, the polarities of ΔV for $I = +0.5$ mA and -0.5 mA are negative and positive, respectively (Fig. 1d). This polarity reversal of ΔV depending on the direction of the bias current $\pm I$ is due to the sign reversal of the spin current at the Au Hall cross. Assuming that the magnetization of FePt is directed upward, the minority (majority) spins of FePt accumulate at the interface for positive (negative) bias current. Therefore, the injected spin current flows in the opposite direction at the Au Hall cross for $\pm I$, resulting in the polarity reversal of ΔV as shown in Fig. 1d. In the V–H curves, the negative and positive voltage offsets appear for $+I$ and $-I$, respectively, which are caused by the electric field applied between terminals A and B, and disappear with increasing d. It is noted that the possibility of enhancement of ΔR_{ISHE} by the AHE in FePt is ruled out because the coefficient of the AHE in FePt is positive and gives ΔV the polarity opposite that of the experimental result. Another striking feature of the present device is the bistable signal at zero magnetic field due to the perpendicular spin injector. From the ISHE signals, α_H of the SHE in Au is determined to be positive.

The temperature dependence of ΔR_{ISHE} is shown in Fig. 2a. ΔR_{ISHE} decreases with decreasing measurement temperature (T). This temperature dependence of ΔR_{ISHE} differs from that for Pt, which shows an increase of spin Hall signals as the temperature decreases[8]. Because of the non-degenerate band dispersion of Au, the large SHE originates from the skew or side-jump scattering mechanisms. Assuming that the interface condition is transparent (metallic contact), ΔR_{ISHE} is phenomenologically expressed as[16]

$$\Delta R_{ISHE} = 2\alpha_H \frac{\rho_{Au}}{t_{Au}} P \exp(-d/\lambda_{Au}),$$

where t_{Au} is the thickness of the Au Hall cross and α_H is the ratio of the spin Hall conductivity to the electrical conductivity. P is the effective current spin polarization and is described as[20]

$$P = \left\{ \frac{p_F}{1-p_F^2} \left(\frac{R_S^{FePt}}{R_S^{Au}} \right) \right\} \Big/ \left\{ 1 + \frac{2}{1-p_F^2} \left(\frac{R_S^{FePt}}{R_S^{Au}} \right) \right\},$$

where p_F is the bulk spin polarization of FePt and $R_s^{FePt(Au)}$ is the spin resistance of FePt (Au). P is found to be ~0.01 assuming $p_F = 0.3$–0.4 (refs 21–23) and using $R_s^{FePt}/R_s^{Au} = 0.04$ (see the Methods section). From the results of ΔR_{ISHE} as a function of d shown in Fig. 2b, λ_{Au} at 295 K is estimated to be 86 ± 10 nm. Consequently, α_H is found to be ~0.113. As mentioned above, α_H is strongly correlated with η_{so}. The dimensionless spin–orbit coupling parameter ($\bar{\eta}_{so}$) is given by[16]

$$\bar{\eta}_{so} = \frac{3\sqrt{3}\pi}{4}\frac{1}{\rho_N \lambda_N}\frac{R_K}{k_F^2},$$

where R_K is the resistance quantum (25.8 kΩ) and k_F is the Fermi momentum of Au ($1.2 \times 10^8\ \mathrm{cm}^{-1}$). In the case of the present Au, $\bar{\eta}_{so}$ is calculated to be 0.3. Surprisingly, α_H for Au (∼0.113) is significantly larger than the value of 0.0037 for Pt (ref. 8). In the case when the side-jump scattering is dominant, $\alpha_H^{SJ} = \eta_{so}/k_F l$, where l is the electron mean free path, is calculated to be $\sim 1.5 \times 10^{-3}$, which is much smaller than the experimental value. On the other hand, α_H of the skew scattering is given by $\alpha_H^{SS} = (2\pi/3)\eta_{so}\langle V_{imp} \cdot N(0)\rangle$, where V_{imp} and $N(0)$ are the impurity potential and the density of states. Using $\alpha_H = 0.113$ and $\bar{\eta}_{so} = 0.3$, $\langle V_{imp} \cdot N(0)\rangle$ is estimated to be 0.18. This small impurity potential is presumably reasonable because the low ρ_{Au} indicates the high purity of the present Au. Therefore, we conclude that the main mechanism causing the large α_H in Au is the skew scattering. α_H weakly depends on temperature (Fig. 2a, inset), which supports that the skew scattering contribution is dominant because α_H^{SJ} decreases with T in contrast with α_H^{SS} not depending on T. We also emphasize that the well-matched R_s leads to highly efficient spin injection. Au and FePt show a better match for R_s compared with a conventional materials combination (see the Methods section), which is an important parameter for the large SHE as well as the large α_H in Au.

The terminal configuration of I^{C-D} and V^{A-B} is used for the detection of the DSHE (Fig. 3a, inset). In this configuration, the FePt spin injector serves as a spin detector for measuring the spin-dependent electrochemical potentials in Au induced by the DSHE (Fig. 3c), which is the same manner as the detection in a conventional non-local spin valve[24,25]. Figure 3a shows the resistance of DSHE ($R_{DSHE} = V^{A-B}/I^{C-D}$) while applying $I = -0.6$ mA, compared with R_{LHE} as a function of H. As in the case of the ISHE, the observed R_{DSHE} follows the magnetization reversal of FePt. ΔR_{DSHE} (2.2 mΩ) is larger than ΔR_{ISHE} (1.15 mΩ). For $I = +0.6$ mA, however, ΔR_{DSHE} is quite small (∼0.3 mΩ). To clarify the reason for the enhancement and reduction of ΔR_{DSHE} for $-I$ and $+I$, respectively, V^{F-A} with I^{C-D} was also measured. Even in this terminal configuration, hysteresis loops of V were observed in both current directions. However, the polarity of ΔV did not depend on the current direction. In addition, ΔV increased as a parabolic function of I. We consider that V^{F-A} with I^{C-D} is the transverse voltage (y direction) in perpendicularly magnetized FePt induced by the heat flow (x direction), which is known as the anomalous Nernst–Ettingshausen effect[26]. As this thermomagnetic effect shows identical voltage polarity regardless of the current direction, we eliminate the extra effect by averaging ΔR_{DSHE}, that is, $\Delta R_{DSHE}^{ave} = (\Delta R_{DSHE}^{+I} + \Delta R_{DSHE}^{-I})/2$. The average ΔR_{DSHE}^{ave} is found to be ∼1 mΩ, which is almost equal to ΔR_{ISHE}. This thermomagnetic effect does not overlap on the ISHE because the Au Hall cross does not have spontaneous magnetization, which was confirmed using the terminal configuration of V^{C-D} and I^{F-A} (see the Supplementary Information).

The variation in R_{DSHE} under a tilted magnetic field with respect to the z direction is shown in Fig. 3b, where the magnetic field is rotated at an angle of ϕ in the z–y plane. No change in R_{DSHE} is observed for $\phi = \pi/2$, and the polarity reversal of R_{DSHE} occurs between $\phi = 0$ and π. For the LHE, DSHE and ISHE, the switching field (H_{sw}) gradually increases with ϕ. The variations in H_{sw} normalized by H_{sw} at $\phi = 0$ follow the $1/\cos\phi$ law (Fig. 3d), supporting that all of the Hall effects are signals from FePt showing magnetization reversal through domain wall propagation. All of the hysteresis loops of the ISHE (Fig. 1) and DSHE (Fig. 3) saturate with the magnetization of FePt, and the ordinary Hall

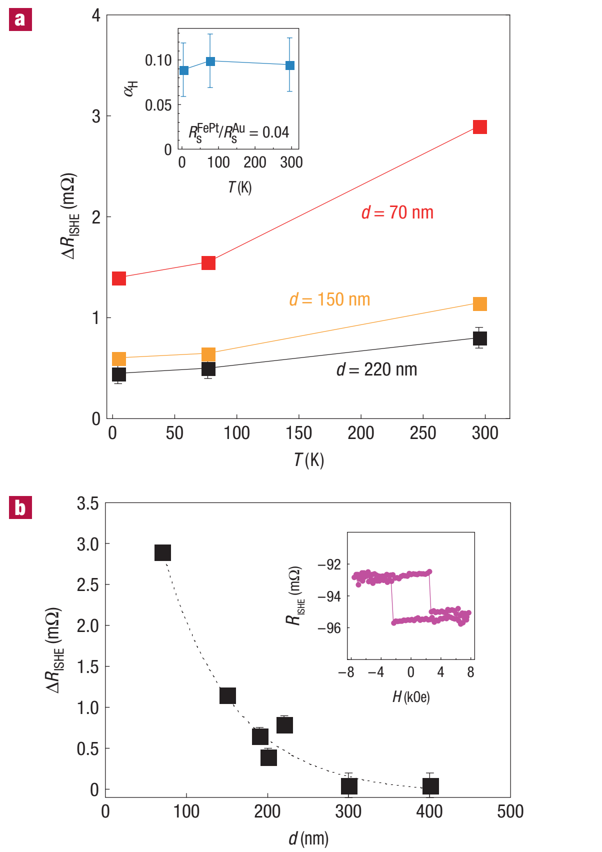

Figure 2 Temperature and distance dependence of ISHE. a, Measurement temperature T dependence of ΔR_{ISHE} for the devices with $d = 70$ nm, 150 nm and 220 nm. Inset: Spin Hall angle α_H as a function of T. The ratio of spin resistances between FePt and Au R_s^{FePt}/R_s^{Au} is fixed at 0.04, and the bulk spin polarization of FePt is assumed to be 0.3–0.4, the range of which gives the error bars of the calculated results. **b**, ΔR_{ISHE} as a function of d measured at 295 K. The dashed curve is the result of an exponential fit to the experimental data. Inset: R_{ISHE} as a function of H for $d = 70$ nm measured at 295 K.

effect induced by the external magnetic field is negligible in the Au Hall cross. In addition, the polarity of R_{ISHE} for I^{F-B} is the same as that for I^{A-B}, which indicates that there is no normal Hall effect owing to the stray field and the non-zero charge current in Au.

A giant ΔR_{ISHE} of 2.9 mΩ is achieved for $d = 70$ nm (Fig. 2b, inset), the magnitude of which is more than 10 times that of previous signals in other non-magnetic metals[6,8]. The SHE signal can be further enhanced by higher current spin polarization using the tunnel spin injection[20,25,27]. We believe that the large SHE in the present multi-terminal device paves the way for SHE-based spin-electronic devices.

METHODS

THIN-FILM PREPARATION

A continuous film with a stacked structure of FePt(10)/Au(10)/Pt(2) (in nanometres) was prepared on a MgO (001) single-crystal substrate using an ultrahigh-vacuum magnetron sputtering system (ULVAC) with high-purity targets of Fe (99.99%), Pt (99.99%) and Au (99.9%). The base pressure was below 1×10^{-9} torr and high-purity argon gas (>99.9999%) was introduced during sputtering. A typical deposition rate was 0.01 nm s^{-1}. First, the FePt layer was epitaxially grown on the MgO substrate heated to 573 K, and subsequently annealed at 773 K to promote the formation of the $L1_0$ ordered structure. The epitaxial growth of the FePt layer with the (001) preferential crystallographic

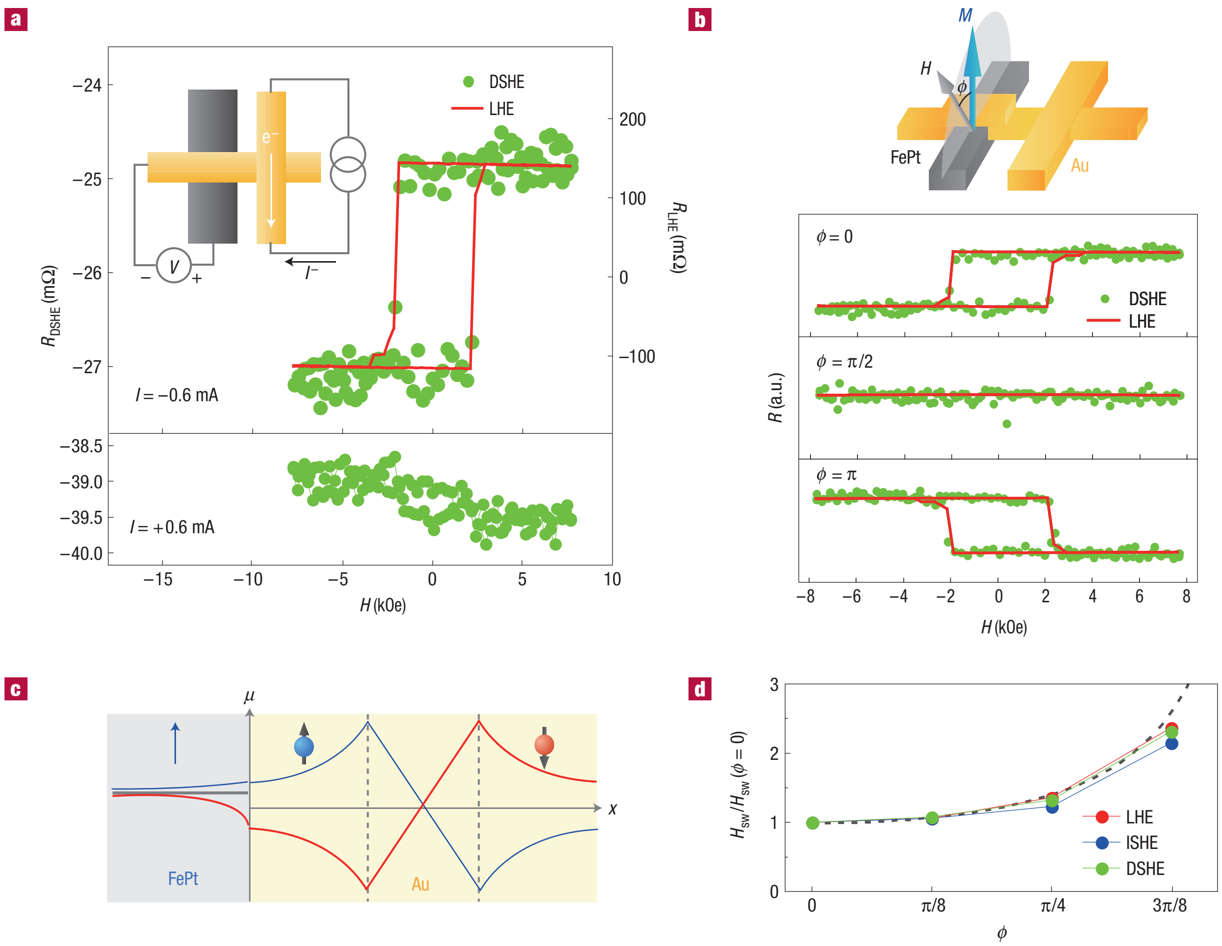

Figure 3 DSHE. **a**, Resistance of DSHE geometry R_{DSHE} versus H for the device with $d = 150$ nm superimposed on R_{LHE} (red lines). The measurement is carried out at room temperature while applying $I = -0.6$ mA (top panel) and $+0.6$ mA (bottom panel). Inset: Schematic diagram of the terminal configuration for the DSHE. **b**, Angular dependence of R_{DSHE} and R_{LHE}. The tilt angle ϕ with respect to the z direction is rotated in the z–y plane. **c**, Spatial map of electrochemical potentials for electrons with up- (blue) and down- (red) spin moments in Au and FePt for the DSHE with negative I. When FePt shows an upward local magnetic moment at a positive H, the electric potential in FePt is lower than that in Au. **d**, Normalized switching field H_{sw} as a function of ϕ for R_{ISHE}, R_{DSHE} and R_{LHE}. H_{sw} is normalized by H_{sw} at $\phi = 0$. The dashed curve denotes the $1/\cos\phi$ law representing magnetization reversal through domain wall motion.

orientation was confirmed by X-ray diffraction. After the deposition of FePt, the substrate was cooled to ambient temperature, and the Au and Pt layers were deposited. The magnetization curve of the continuous film, which was measured using a superconducting quantum interference device magnetometer and the polar magneto-optical Kerr effect, showed strong perpendicular magnetic anisotropy. An important point in the present thin-film preparation is that the interface between the FePt and Au was formed in an ultrahigh-vacuum condition before the microfabrication process, which enabled us to keep the interface clean as it was not exposed to air during microfabrication.

DEVICE FABRICATION AND ELECTRICAL MEASUREMENT

Instead of a conventional lift-off process, an ion etching process was used for device fabrication. A negative-type electron beam resist (Tokyo Ohka Kogyo) was spin-coated on the continuous film, and was patterned into the shape of the FePt spin injector using electron beam lithography (ELS-7500, ELIONIX). After patterning of the electron beam resist, the continuous film was completely etched by argon ions through the resist mask. Subsequently, the patterned sample was returned to the ultrahigh-vacuum sputtering chamber to deposit a 10-nm-thick Au layer on the sample surface. Finally, the Au layer was patterned into the shape of the Hall cross by electron beam lithography and ion etching. The ion etching was monitored by secondary-ion mass spectroscopy.

The device resistance was simply measured by a nanovoltmeter (34401A, Agilent) while applying a d.c. current. The external magnetic field was applied perpendicularly to the sample plane. Measurements were carried out at 295 K, 77 K and 4.2 K.

CALCULATION OF SPIN RESISTANCE

The spin resistance R_s is given by $R_s = (\rho\lambda)/A$, where ρ, λ and A are the resistivity, the spin diffusion length and the effective cross-sectional area, respectively. R_s^{Au} is found to be 1.62 Ω with $A_{Au} = 1.5 \times 10^{-15}$ m^2 (thickness × width). In the case of R_s^{FePt}, on the other hand, the current distribution should be taken into account because of the short $\lambda_{FePt} \sim 5$ nm, which is estimated from the current-perpendicular-to-plane giant magnetoresistance in the FePt layers. Using $A_{FePt} = 3 \times 10^{-14}$ m^2 (contact area between FePt and Au), R_s^{FePt} is found to be 0.06 Ω. Therefore, R_s^{FePt}/R_s^{Au} is 0.04.

Note that the ratio of $\rho_{FePt}\lambda_{FePt}$ to $\rho_{Au}\lambda_{Au}$ is quite high (0.7) compared with that of a conventional materials combination, for example, $\rho_{Py}\lambda_{Py}/\rho_{Cu}\lambda_{Cu} \sim 0.04$ for permalloy (Py) and Cu, where the values reported in ref. 8 are used to calculate Py/Cu and A is not taken into account because it depends on the device geometry and size. These calculations indicate that the combination of FePt and Au is well suited for highly efficient spin injection.

Received 5 July 2007; accepted 30 November 2007; published 13 January 2008.

References

1. Kato, Y. K., Myers, R. C., Gossard, A. C. & Awschalom, D. D. Observation of the spin Hall effect in semiconductors. *Science* **306**, 1910–1913 (2004).

2. Wunderlich, J., Kaestner, B., Sinova, J. & Jungwirth, T. Experimental observation of the spin-Hall effect in a two-dimensional spin–orbit coupled semiconductor system. *Phys. Rev. Lett.* **94**, 047204 (2005).
3. Sih, V. *et al.* Spatial imaging of the spin Hall effect and current-induced polarization in two-dimensional electron gases. *Nature Phys.* **1**, 31–35 (2005).
4. Zhao, H., Loren, E. J., van Driel, H. M. & Smirl, A. L. Coherent control of Hall charge and spin currents. *Phys. Rev. Lett.* **96**, 246601 (2006).
5. Stern, N. P. *et al.* Current-induced polarization and the spin Hall effect at room temperature. *Phys. Rev. Lett.* **97**, 126603 (2006).
6. Valenzuela, S. O. & Tinkham, M. Direct electronic measurement of the spin Hall effect. *Nature* **442**, 176–179 (2006).
7. Saitoh, E., Ueda, M., Miyajima, H. & Tatara, G. Conversion of spin current into charge current at room temperature: Inverse spin-Hall effect. *Appl. Phys. Lett.* **88**, 182509 (2006).
8. Kimura, T., Otani, Y., Sato, T., Takahashi, S. & Maekawa, S. Room-temperature reversible spin Hall effect. *Phys. Rev. Lett.* **98**, 156601 (2007).
9. Dyakonov, M. I. & Perel, V. I. Current-induced spin orientation of electrons in semiconductors. *Phys. Lett. A* **35**, 459–460 (1971).
10. Hirsch, J. E. Spin Hall effect. *Phys. Rev. Lett.* **83**, 1834–1837 (1999).
11. Zhang, S. Spin Hall effect in the presence of spin diffusion. *Phys. Rev. Lett.* **85**, 393–396 (2000).
12. Murakami, S., Nagaosa, N. & Zhang, S. Dissipationless quantum spin current at room temperature. *Science* **301**, 1348–1351 (2003).
13. Sinova, J. *et al.* Universal intrinsic spin Hall effect. *Phys. Rev. Lett.* **92**, 126603 (2004).
14. Inoue, J., Bauer, G. E. W. & Molenkamp, L. W. Suppression of the persistent spin Hall current by defect scattering. *Phys. Rev. B* **70**, 041303 (2004).
15. Shchelushkin, R. V. & Brataas, A. Spin Hall effects in diffusive normal metals. *Phys. Rev. B* **71**, 045123 (2005).
16. Takahashi, S., Imamura, H. & Maekawa, S. in *Concepts in Spin Electronics* (ed. Maekawa, S.) (Oxford Univ. Press, Oxford, 2006).
17. Wolf, S. A. *et al.* Spintronics: A spin-based electronics vision for the future. *Science* **294**, 1488–1495 (2001).
18. Chien, C. L. & Westgate, C. R. (eds) *The Hall Effect and Its Applications* (Plenum, New York, 1980).
19. Kondo, J. Anomalous Hall effect and magnetoresistance of ferromagnetic metals. *Prog. Theor. Phys.* **27**, 772–791 (1962).
20. Takahashi, S. & Maekawa, S. Spin injection and detection in magnetic nanostructures. *Phys. Rev. B* **67**, 052409 (2003).
21. Kaiser, C., van Dijken, S., Yang, S.-H., Yang, H. & Parkin, S. S. P. Role of tunneling matrix elements in determining the magnitude of the tunneling spin polarization of 3d transition metal ferromagnetic alloys. *Phys. Rev. Lett.* **94**, 247203 (2005).
22. Mitani, S., Tsukamoto, K., Seki, T., Shima, T. & Takanashi, K. Fabrication and characterization of $L1_0$-ordered FePt/AlO/FeCo magnetic tunnel junctions. *IEEE Trans. Magn.* **41**, 2606–2608 (2005).
23. Seki, T., Mitani, S., Yakushiji, K. & Takanashi, K. Spin-polarized current-induced magnetization reversal in perpendicularly magnetized $L1_0$-FePt layers. *Appl. Phys. Lett.* **88**, 172504 (2006).
24. Jedema, F. J., Filip, A. T. & van Wees, B. J. Electrical spin injection and accumulation at room temperature in an all-metal mesoscopic spin valve. *Nature* **410**, 345–348 (2001).
25. Jedema, F. J., Heersche, H. B., Filip, A. T., Baselmans, J. J. A. & van Wees, B. J. Electrical detection of spin precession in a metallic mesoscopic spin valve. *Nature* **416**, 713–716 (2002).
26. Seitz, F. & Turnbull, D. (eds) *Solid State Physics* (Academic, New York, 1957).
27. Valenzuela, S. O. & Tinkham, M. Spin-polarized tunneling in room-temperature mesoscopic spin valves. *Appl. Phys. Lett.* **85**, 5914–5916 (2004).

Acknowledgements

This work was partially supported by the Industrial Technology Research Grant Program in 2005 from NEDO. The device fabrication was partly carried out at the Advanced Research Center of Metallic Glasses, IMR, Tohoku University. The authors thank G. E. W. Bauer, E. Saitoh and M. Mizuguchi for their helpful comments and critical reading of this manuscript.

Correspondence and requests for materials should be addressed to T.S.

Supplementary Information accompanies this paper on www.nature.com/naturematerials.

Author contributions

T.S. played the primary role in carrying out the sample preparation and the measurement. Y.H. assisted in the sample preparation and the measurement. The third author, S.T. and H.I. contributed to the theoretical modelling for the interpretation and the data analyses. All of the authors contributed to the physical understanding, the data analysis and the preparation of the manuscript.